SEGUE: a Speedy rEgion-Growing algorithm for Unwrapping Estimated phase

Anita Karsa[1] and Karin Shmueli[1]

[1]Department of Medical Physics and Biomedical Engineering, University College London, London, United Kingdom

Synopsis

MRI phase images are increasingly used, for example for Susceptibility Mapping, and distortion correction in functional and diffusion MRI. However, measured phase images contain wraps, because the phase is defined only between 0 and 2π. PRELUDE is the current gold-standard method for robust, 3D, spatial phase unwrapping, but its computation time can become very long (e.g. 10 hours), especially at high field and outside the brain. Here, we developed a new method, SEGUE, that produced similar results to PRELUDE in multi-echo brain and head-and-neck images, successfully unwrapped some regions where PRELUDE failed and was between 1.6 and 83 times faster.

Purpose

A range of MRI techniques, including susceptibility mapping[1-3], have recently been developed that exploit the phase component of the complex MR signal. Moreover, phase images are often used for distortion correction in functional[4-9] and diffusion[10-12] MRI. However, the MRI phase is only defined between 0 and 2π, resulting in phase wraps. Phase Region Expanding Labeller for Unwrapping Discrete Estimates[13-14] (PRELUDE) is the gold standard method for robust, spatial phase unwrapping in 3D[15]. However, the computation time (T_c) increases with field strength, echo time and outside the brain. To accelerate phase unwrapping for these applications, we developed a **S**peedy r**E**gion-**G**rowing algorithm for **U**nwrapping **E**stimated phase (**SEGUE**) based on similar principles to PRELUDE.

Theory

In PRELUDE[13-14], the phase map is partitioned into connected regions by dividing the [0, 2π] interval into 6 smaller, equal intervals. These regions are then unwrapped and merged by adding integer multiples of 2π to one of two neighbouring regions assuming spatial smoothness of the phase. This process continues until all the regions are merged. T_c increases with the number of initial regions. In high-resolution images, a single region can erroneously contain a wrap if it consists of areas with phase difference > 2π connected by a few noisy voxels. To avoid this, PRELUDE limits the initial regions to be 2D for high-resolution images (voxel size < 1 mm). This increases the number of initial regions and, consequently, T_c.

In SEGUE, we first divide the [0, 2π] interval into 6 intervals (similarly to PRELUDE) to determine the initial regions. Instead of restricting the regions to be 2D, small bridges of a few voxels between larger areas are removed before partitioning to avoid wraps within the 3D regions (Figure 1). The region with the largest border (R_m) is then selected and all the adjacent regions (R_a) that meet the following criteria are simultaneously unwrapped and merged with R_m: 1. The border between R_m and R_a is greater than P = 30% of the entire border of R_a. 2. A substantial proportion of neighbouring voxel pairs in R_m and R_a agree on the phase difference between R_m and R_a. When no more regions can be merged with R_m, a new R_m is selected and this process is repeated until at least 70% of the tissue mask is unwrapped. The entire merging process is repeated with P = 10% and P = 0% respectively.

Methods

Brain and head-and-neck images of two healthy volunteers were acquired on a 3-T Philips Achieva system (Best, NL) with parameters shown in Figure 1. All phase images were unwrapped using both PRELUDE and SEGUE (the latter implemented in Matlab R2015a) and the results were compared using: 1. T_c on a 64-bit Ubuntu Virtual Machine with a 3.5 GHz Processor and 16 GB RAM 2. Histograms of the unwrapped phase (SEGUE–PRELUDE) difference images within the brain mask (obtained using FSL BET[16] on the last-echo magnitude image) or within the tissue mask (obtained by thresholding the inverse noise map of the head-and-neck images[17-18]). Both techniques failed to unwrap the second-echo head-and-neck phase image, therefore, in this we applied them separately in fat and water masks. Fat-water separation was performed on the multi-echo head-and-neck data using the 3-point Dixon method[19] from the ISMRM fat-water separation toolbox[20].

Results and Discussion

Figures 2 and 3 show comparisons of PRELUDE and SEGUE for all echoes in the brain and head-and-neck images respectively. For PRELUDE, T_c increased greatly at later echoes, while T_c for SEGUE was similar across echoes. SEGUE was 1.6 to 83 times faster than PRELUDE. The vast majority of voxels had the same phase value following PRELUDE or SEGUE (Figures 2 and 3 d). In the head-and-neck images, most of the ±2π differences between the unwrapped maps were found around the nasal septum (Figure 4) which is connected to the bulk of the tissue by only a few voxels making it difficult to estimate its phase. There were more ±2π differences in the second-echo head-and-neck images where both techniques failed due to the additional, chemical shift-induced phase in the fatty tissue (Figure 3, green arrows). Applying the two methods separately in fat and water masks solved this problem (Figure 3, blue arrows). The red arrows in Figures 2 and 3 indicate regions where PRELUDE failed and SEGUE succeeded.

Conclusions

We have developed and tested SEGUE, a spatial phase unwrapping technique that was between 1.6 and 83 times faster than PRELUDE, and produced very similar results, successfully unwrapping some regions where PRELUDE failed. SEGUE is useful for rapid, robust, and accurate unwrapping of highly wrapped phase images.

Acknowledgements

Anita Karsa's work was supported by the EPSRC-funded UCL Centre for Doctoral Training in Medical Imaging (EP/L016478/1) and the Department of Health's National Institute for Health Research funded Biomedical Research Centre at University College London Hospitals. Karin Shmueli was supported by an EPSRC First Grant (EP/K02746/1).

References

1. Shmueli, Karin, et al. "Magnetic susceptibility mapping of brain tissue in vivo using MRI phase data." Magnetic resonance in medicine 62.6 (2009): 1510-1522.

2. Reichenbach, J. R., et al. "Quantitative susceptibility mapping: concepts and applications." Clinical neuroradiology 25.2 (2015): 225-230.

3. Eskreis-Winkler, Sarah, et al. "The clinical utility of QSM: disease diagnosis, medical management, and surgical planning." NMR in Biomedicine 30.4 (2017).

4. Klein, Tilmann A., Markus Ullsperger, and Gerhard Jocham. "Learning relative values in the striatum induces violations of normative decision making." Nature Communications 8 (2017).

5. Brooks, Jonathan CW, Wendy-Elizabeth Davies, and Anthony E. Pickering. "Resolving the Brainstem Contributions to Attentional Analgesia." Journal of Neuroscience 37.9 (2017): 2279-2291.

6. Cardoso, Pedro Lima, et al. "The clinical relevance of distortion correction in presurgical fMRI at 7T." NeuroImage (2016).

7. Branco, Paulo, Daniela Seixas, and São Luís Castro. "Temporal reliability of ultra-high field resting-state MRI for single-subject sensorimotor and language mapping." NeuroImage (2016).

8. Ashburner, John. "Preparing fMRI Data for Statistical Analysis." fMRI Techniques and Protocols (2016): 155-181.

9. Ahveninen, Jyrki, et al. "Intracortical depth analyses of frequency-sensitive regions of human auditory cortex using 7TfMRI." NeuroImage 143 (2016): 116-127.

10. Shen, Kaikai, et al. "A spatio-temporal atlas of neonatal diffusion MRI based on kernel ridge regression." Biomedical Imaging (ISBI 2017), 2017 IEEE 14th International Symposium on. IEEE, 2017.

11. Herting, Megan M., et al. "Longitudinal changes in pubertal maturation and white matter microstructure." Psychoneuroendocrinology 81 (2017): 70-79.

12. Rajagopalan, Venkateswaran, and Erik P. Pioro. "Differential involvement of corticospinal tract (CST) fibers in UMN-predominant ALS patients with or without CST hyperintensity: A diffusion tensor tractography study." NeuroImage: Clinical 14 (2017): 574-579.

13. Jenkinson, Mark. "Fast, automated, N-dimensional phase-unwrapping algorithm." Magnetic resonance in medicine 49.1 (2003): 193-197.

14. FSL Prelude: http://fsl.fmrib.ox.ac.uk/fsl/fslwiki/FUGUE

15. Robinson, Simon Daniel, et al. "An illustrated comparison of processing methods for MR phase imaging and QSM: combining array coil signals and phase unwrapping." NMR in Biomedicine 30.4 (2017).

16. Smith, Stephen M. "Fast robust automated brain extraction." Human brain mapping 17.3 (2002): 143-155.

17. Kressler, Bryan, et al. "Nonlinear regularization for per voxel estimation of magnetic susceptibility distributions from MRI field maps." IEEE transactions on medical imaging 29.2 (2010): 273.

18. MEDI toolbox: http://weill.cornell.edu/mri/pages/qsm.html

19. Berglund, Johan, et al. "Three-point dixon method enables whole-body water and fat imaging of obese subjects." Magnetic Resonance in Medicine 63.6 (2010): 1659-1668.

20. ISMRM fat-water separation toolbox: https://www.ismrm.org/workshops/FatWater12/data.htm

21. Marques, J. P., and R. Bowtell. "Application of a Fourier-based method for rapid calculation of field inhomogeneity due to spatial variation of magnetic susceptibility." Concepts in Magnetic Resonance Part B: Magnetic Resonance Engineering 25.1 (2005): 65-78.

22. Zubal, I. George, et al. "Two dedicated software, voxel-based, anthropomorphic (torso and head) phantoms." Proceedings of the International Workshop, National Radiological Protection Board, Chilton, UK. Vol. 6. No. 7. 1995.

23. Karsa, Anita, et al. "Resolution and Coverage for Accurate Susceptibility Maps: Comparing Brain Images with Simulations." Proceedings of the 25th Annual Meeting of the ISMRM, Honolulu. 2017. p. 3677

Figures

	Brain images	Head-and-neck images
Sequence	3D GRE	3D GRE
Coil	32-channel head coil	16-channel head-and-neck coil
Matrix size	240×240×144	220×240×240
SENSE factor	1×2×1.5	1.5×2×1
Resolution	1 mm isotropic	1 mm isotropic
TE_1	3 ms	3 ms
ΔTE	5.4 ms	5.3 ms
Number of echoes	5	4
TR	29 ms	23 ms
Flip angle	20°	18°

Figure 1: MRI acquisition parameters used to acquire multi-echo brain and head-and-neck images to test and compare SEGUE with PRELUDE.

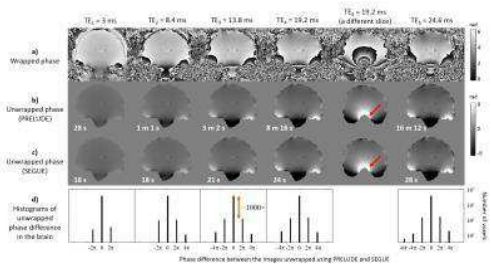

Figure 2: Brain phase maps at 5 echo times before unwrapping (a), and after unwrapping using PRELUDE (b) or SEGUE (c). T_c is shown next to the unwrapped images. The histograms of the SEGUE–PRELUDE unwrapped phase difference maps (d) are also shown on a logarithmic scale. There were 1000 times fewer voxels with ±2π than 0 phase differences (orange double arrow). The red arrows indicates where PRELUDE failed but SEGUE succeeded to unwrap (by visual comparison).

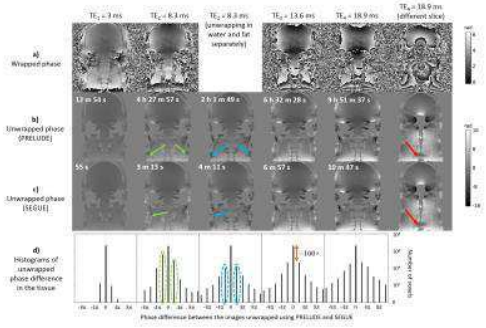

Figure 3: Head-and-neck phase maps at 4 echo times before unwrapping (a), and after unwrapping using PRELUDE (b) or SEGUE (c). T_c is shown next to the unwrapped images. Histograms of the SEGUE–PRELUDE unwrapped phase difference maps (d) are also shown (logarithmic scale). There were 100 times fewer voxels with ±2π than 0 phase differences (orange arrow). The red arrows indicates where PRELUDE failed but SEGUE succeeded. Both techniques failed in the second-echo phase images (green arrows) in fatty tissue due to chemical shift effects. Applying both techniques separately in the water and fat masks solved this problem (blue arrows).

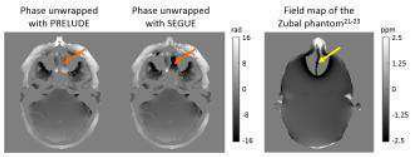

Figure 4: Last-echo (TE_4 = 18.9 ms) phase images unwrapped using PRELUDE and SEGUE. The orange arrows indicate the soft tissue around the nasal septum which is connected to the bulk of the tissue by only a few voxels. This led to different unwrapped phase values for the two techniques. The SEGUE result seems more accurate as it is more similar to the field map calculated by applying a Fourier-based forward model[21] to the Zubal phantom[22-23] (yellow arrow).